

Learning to be EXACT

Cell Detection for Asthma on Partially Annotated Whole Slide Images

Christian Marzahl^{1,2}, Christof A. Bertram³, Frauke Wilm¹, Jörn Voigt²,
Ann K. Barton⁴, Robert Klopffleisch³, Katharina Breininger¹, Andreas Maier¹,
Marc Aubreville⁵

¹Pattern Recognition Lab, Department of Computer Science,
Friedrich-Alexander-Universität Erlangen-Nürnberg (FAU), Germany

²R & D Projects, EUROIMMUN Medizinische Labordiagnostika AG

³Institute of Veterinary Pathology, Freie Universität Berlin, Germany

⁴Equine Clinic, Freie Universität Berlin, Berlin, Germany

⁵Technische Hochschule Ingolstadt, Ingolstadt, Germany

c.marzahl@euroimmun.de

Abstract. Asthma is a chronic inflammatory disorder of the lower respiratory tract and naturally occurs in humans and animals including horses. The annotation of an asthma microscopy whole slide image (WSI) is an extremely labour-intensive task due to the hundreds of thousands of cells per WSI. To overcome the limitation of annotating WSI incompletely, we developed a training pipeline which can train a deep learning-based object detection model with partially annotated WSIs and compensate class imbalances on the fly. With this approach we can freely sample from annotated WSIs areas and are not restricted to fully annotated extracted sub-images of the WSI as with classical approaches. We evaluated our pipeline in a cross-validation setup with a fixed training set using a dataset of six equine WSIs of which four are partially annotated and used for training, and two fully annotated WSI are used for validation and testing. Our WSI-based training approach outperformed classical sub-image-based training methods by up to 15% *mAP* and yielded human-like performance when compared to the annotations of ten trained pathologists.

1 Introduction

Asthma is a chronic inflammatory disorder of the lower respiratory tract and can occur in multiple species. While asthma can affect humans, horses can also suffer from asthma and are often used as models for human disease [1] due to their similar symptoms and pathogenesis. The gold standard for diagnosis of equine and human asthma is to collect bronchoalveolar lavage fluid (BALF) and to examine the sample under a microscope or on digitised whole slide images (WSIs). Asthma and other pulmonary disorders are diagnosed based on the relative proportion

of different cell types including eosinophils, mast cells, neutrophils, macrophages and lymphocytes. This typically requires manual counting of 300-500 cells and is therefore time-consuming and strenuous for the pathologist [2]. Therefore, automatic solutions that support this task are of high interest. Although asthma is a common disease in horses and humans, to the author’s knowledge there is no trained model or method published analysing asthma on WSI automatically. For the development of machine learning algorithms, huge annotated datasets are generally required. A particular challenge for the annotation process of asthma is the large number of cells per WSI, which can easily reach hundreds of thousands. This makes the annotation process very labour-intensive and time-consuming. In order to increase the efficiency of the annotation process, expert-algorithm collaboration can be used where experts enhance pre-computed annotations of a trained model. Marzahl et al.[2] showed this for mitotic figures or pulmonary haemorrhage. An alternative option is to annotate multiple WSIs only partially to capture the domain variability between WSIs, and train a network to complete the annotation. On the one hand, training deep learning-based methods on partially annotated WSIs faces some additional challenges regarding tracking annotated WSI areas and leads to higher demands on the coordination and synchronisation between the participating institutes. On the other hand, training on partially annotated data simplifies training pipelines in terms of data augmentation and live patch sampling in contrast to extracted sub-image-based approaches. Nevertheless, sub-image-based approaches, where patches from the WSI have to be extracted before the training, are the only supported method for the most prominent object detection frameworks [3] and are used in multiple WSI-based detection applications [4,5].

As the main contribution to the field of deep learning-based cytological WSI analysis, we propose a training pipeline to train object detection models with live sampling on partially annotated WSIs. Additionally, we create a baseline with a state-of-the-art deep learning-based object detection model for detecting five types of cells on WSIs. All code to train, evaluate, test our models and to reproduce our results for public is accessible at GitHub¹. Furthermore, the WSIs can be accessed at reasonable request from the corresponding author.

2 Material and methods

The dataset consists of six cytological samples (Table 1) of equine BALF which were cytocentrifugated and stained using May-Grunwald Giemsa stain. Afterwards, the glass slides were digitized using a linear scanner (Aperio ScanScope CS2, Leica Biosystems, Germany) at a magnification of $400\times$ with a resolution of $0.25 \frac{\mu m}{px}$. Finally, two slides were completely annotated and the remaining four partially annotated by a veterinary pathologist. Twenty patches from the same six WSI have been used in a recent study [2] to investigate the annotation accuracy from ten trained pathologist. We exclude these twenty patches

¹ https://github.com/ChristianMarzahl/Asthma_WSI

Table 1. Overview of the dataset including the file id, the number of cells per type and the screened sample area. The top two rows represent the completely annotated validation and test slides for the cross validation with a fixed train set.

| id | eosinophils | mast cells | neutrophils | macrophages | lymphocytes | total | screened image |
|----|-------------|------------|-------------|-------------|-------------|-------|----------------|
| 1 | 21 | 511 | 3301 | 3934 | 14846 | 22613 | 100% |
| 2 | 47 | 762 | 951 | 16748 | 10342 | 28850 | 100% |
| 3 | 10 | 69 | 1321 | 3081 | 15666 | 20147 | 8% |
| 4 | 20 | 37 | 2467 | 729 | 2144 | 5397 | 28% |
| 5 | 8 | 116 | 4491 | 1639 | 3077 | 9331 | 43% |
| 6 | 2 | 40 | 26 | 370 | 323 | 761 | 1% |
| | 108 | 1535 | 12557 | 26501 | 46398 | 87099 | 46% |

from training to compare the accuracy of human experts with our algorithmic approach.

2.1 Label generation and training pipeline

The dataset containing only six WSIs appears to be comparably small. However, the cells in the WSIs are annotated by experts and subdivided into five classes using SlideRunner [6], rendering it one of the largest manually annotated cytology datasets to date. The dataset displays an extreme class imbalance, with the

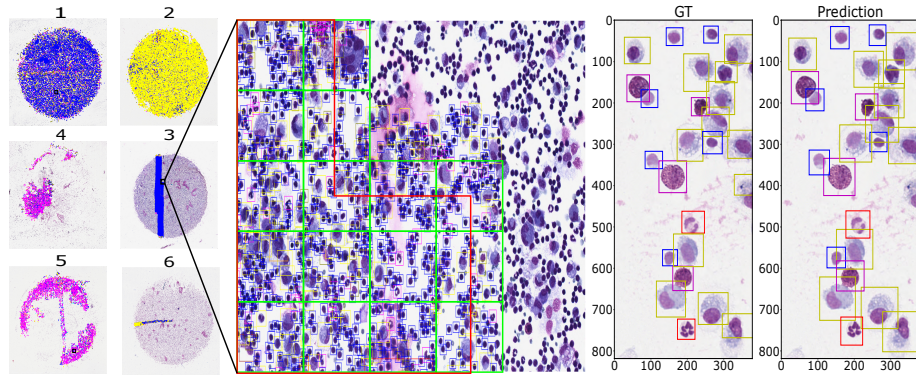


Fig. 1. Left: visualisation of the annotated regions/cells of the included slides. Center: visualisation of the 16 traditional fully annotated sub-images for sampling in green and 624 cell-based sampling positions for our live sampling approach within the red area. To prevent sampling from unannotated WSI areas, the red area is restricted to half of the patch size to the annotation border. Right: The ground truth (GT) and the deep learning based predictions; neutrophils (red), eosinophils (green), lymphocytes (blue), macrophages (yellow), mast cells (purple).

rarest class of eosinophils representing only 0.12% of all annotations. A particular challenge for training neuronal networks emerges from the sparse annotation of four WSIs, as shown in the column "screened" in table 1. To meet this challenge of partially annotated WSIs, we apply an online training approach using the open-source online annotation platform EXACT [7]. EXACT supports a persistent screening mode that allows experts to screen WSIs in a self-determined resolution. By reusing the information this screening mode provides, we are able to track exactly which areas of the slide have already been annotated by the expert and can download them into the training process via the provided REST-API.

We propose the following online training pipeline for equine asthma. As a first step, screened areas of the slides and associated annotations are downloaded from the EXACT server via the REST-API. The training pipeline is then initialised with the downloaded information, the network architecture and the loss function. During training, new patches are sampled live from the WSI according to the patch selection and sampling strategy described in the following sections and are restricted by information about the screened area provided by EXACT. The trained models can be applied to new data and the results can be synchronised with the server for expert review.

2.2 Live patch selection and sampling strategy

To counteract the described class imbalance and partial annotations, we propose the following sampling strategy which uses annotated cells as seeds for training patches: Each training patch has a cell that was manually annotated by an expert in its center. Consequently, only cells that have at least a distance of half of the patch size to the border of the annotated region can be used as patch centers (red area in Figure 1). Each training batch contains at least five patches with each of the five cell types represented as patch center cell. The center cells within each class are randomly chosen from the annotations. If the training batch size is chosen larger than the number of cell types, a new cell type is randomly selected with a probability proportional to $1 - p_k$ where p_k is the relative class frequency of each cell type until the required batch size is reached. This results in a sampling strategy which can freely choose the sampled patches and reduces the possibility of sampling a given region repeatedly. This is highly desirable to counter overfitting and works as an advanced augmentation technique.

For comparison we extract all available fully annotated areas as sub-images of the WSIs to simulate a traditional training pipeline. This results in a total of 1862 sub-images of which 851 belong to the two fully annotated test WSIs. Example sub-images are visualised in Figure 1 on the right with green rectangles. For training the same cell type-based sampling strategy to counteract the described class imbalance is applied.

2.3 Object detection methods

Since the training strategy itself is the main contribution of this work, we use a publicly available and for cytology optimised implementation [8] of the success-

Table 2. The mean average precision for the five types of cells in respect to the number of layers used for the ResNet backbone network (BB) and batch size (BS). The modes represent our method working on partially annotated WSIs and a classical approach with extracted sub-images.

| mode | BB | BS | eosinophils | mast cell | neutrophils | macrophages | lymphocytes | \varnothing |
|-----------|----|----|-------------|-----------|-------------|-------------|-------------|---------------|
| ours | 18 | 16 | 0.93 | 0.85 | 0.88 | 0.89 | 0.81 | 0.87 |
| sub-image | 18 | 16 | 0.69 | 0.72 | 0.68 | 0.80 | 0.71 | 0.72 |
| ours | 34 | 16 | 0.91 | 0.86 | 0.90 | 0.89 | 0.78 | 0.87 |
| sub-image | 34 | 16 | 0.70 | 0.71 | 0.68 | 0.80 | 0.72 | 0.72 |
| ours | 50 | 6 | 0.92 | 0.80 | 0.90 | 0.89 | 0.81 | 0.86 |
| sub-image | 50 | 6 | 0.72 | 0.69 | 0.68 | 0.81 | 0.75 | 0.73 |

ful RetinaNet [9] architecture. Different ResNet-variants [10] (ResNet-18, -34, -50) pretrained on ImageNet are applied as backbone networks with appropriate mini-batch sizes. The networks are trained using the sub-images-based and the proposed live sampling-based approach with a patch size of 1024×1024 px. Each of the two fully annotated WSIs (Table 1) are used once as the validation set and once as the test set while keeping the training set static to allow for a form of cross-validation given the limited amount of cases. During training, data augmentation (rotation between zero and 90 degrees, horizontal and vertical flips, random increase or decrease of intensity in the range of -20 to +20%) is applied and the networks are trained until convergence on the validation set. The initial learning rate is set to 1e-3 and reduced to 1e-4 and 1e-5 if the validation loss doesn't decrease for three epochs. One epoch consists of 500 training patches regardless of the WSI-based sampling mode or the extracted sub-images. The object detection accuracy is measured as mean Average Precision (mAP) according to the 2007 PASCAL VOC challenge.

3 Results

Independent of the backbone model or batch size, the accuracy of our WSI-based sampling approach converge at an mAP of 0.87 (min=0.86, max=0.87, IoU=0.5, epochs=73), outperforming the model trained on sub-images (mAP=0.72, min = 0.72, max=0.73, IoU=0.5, epochs=23) as shown in Table 2. After 23 epochs the sub-images-based training is terminated due to overfitting. The backbone network of the model has no effect on the accuracy. The live sampling approaches show the lowest performance for the lymphocytes, which are the smallest and most clustered type of cells. The sub-images-based approach scores lowest on the rare classes of eosinophils and mast cells due to overfitting.

When applying the trained solution with a ResNet-18 as a backbone on the image patches and ground-truth published in [blinded for peer review], we reach a mean mAP across images of 0.76 with the proposed method and 0.63 with the sub-images-based approach compared to the experts reaching a published mean concordance of $\mu=0.73$ mAP (min=0.56, max=0.82, $\sigma=0.08$).

4 Discussion and outlook

We demonstrated the creation of an object detection training pipeline which is able to use partially annotated WSIs efficiently and is superior to a simple sub-image-based approach. Our proposed approach allows for better sampling strategies and data augmentation for rare classes which massively reduces the chance to sample the same patch repeatedly and therefore mitigate overfitting, as apparent in the considerable difference in performance for eosinophils in the evaluation. This resulted in a object detection model with human like performance on a small set of example patches. However, this work has the limitation that only six images have been partially annotated by one expert, which needs to be addressed in further research. This work can be used as a baseline for further enhancements, like increasing the detection performance of small cells, optimising the non-maximum suppression algorithm for high quantities of cells but also to create new annotations in an expert-algorithm based manner on the remaining WSIs.

Acknowledgement. CAB gratefully acknowledges financial support received from the Dres. Jutta & Georg Bruns-Stiftung für innovative Veterinärmedizin.

References

1. Bullone M, Lavoie JP. Asthma “of horses and men”—how can equine heaves help us better understand human asthma immunopathology and its functional consequences? *Mol Immunol.* 2015;66(1):97–105.
2. Marzahl C, Bertram CA, Aubreville M, et al. Are Fast Labeling Methods Reliable? A Case Study of Computer-Aided Expert Annotations on Microscopy Slides. In: MICCAI. Cham: Springer International Publishing; 2020. p. 24–32.
3. Huang J, Rathod V, Sun C, et al. Speed/accuracy trade-offs for modern convolutional object detectors. In: CVPR; 2017. p. 7310–7311.
4. Kawazoe Y, Shimamoto K, Yamaguchi R, et al. Faster r-cnn-based glomerular detection in multistained human whole slide images. *Imaging.* 2018;4(7):91.
5. Yang F, Yu H, Silamut K, et al. Parasite Detection in Thick Blood Smears Based on Customized Faster-RCNN on Smartphones. In: AIPR; 2019. p. 1–4.
6. Aubreville M, Bertram C, Klopffleisch R, et al. SlideRunner. In: *Bildverarbeitung für die Medizin 2018.* Springer; 2018. p. 309–314.
7. Marzahl C, Aubreville M, Bertram CA, et al. EXACT: A collaboration toolset for algorithm-aided annotation of almost everything. *arXiv preprint arXiv:200414595.* 2020;.
8. Marzahl C, Aubreville M, Bertram CA, et al. Deep Learning-Based Quantification of Pulmonary Hemosiderophages in Cytology Slides. *Sci Rep.* 2020;10(1):1–10.
9. Lin TY, Goyal P, Girshick R, et al. Focal loss for dense object detection. In: *Proceedings of the IEEE international conference on computer vision;* 2017. p. 2980–2988.
10. He K, Zhang X, Ren S, et al. Deep residual learning for image recognition. In: *CVPR;* 2016. p. 770–778.